AIAA 2005-0099

THREE-DIMENSIONAL WAVE PACKET IN A HYPERSONIC BOUNDARY LAYER

Eric Forgoston* and Anatoli Tumin†
The University of Arizona, Tucson, AZ 85721

Abstract

A three-dimensional wave packet generated by a local disturbance in a hypersonic boundary layer flow is studied with the aid of the previously solved initial-value problem. The solution to this problem can be expanded in a biorthogonal eigenfunction system as a sum of discrete and continuous modes. A specific disturbance consisting of an initial temperature spot is considered, and the receptivity to this initial temperature spot is computed for both the two-dimensional and three-dimensional cases. Using previous analysis of the discrete and continuous spectrum, we numerically compute the inverse Fourier transform. The two-dimensional inverse Fourier transform is found for Mode S, and the result is compared with the asymptotic approximation of the Fourier integral. Due to the synchronism between Mode F and entropy/vorticity modes, it is necessary to deform the path of integration around the associated branch cut. Additionally, the inverse Fourier transform for a prescribed spanwise wave number is computed for three-dimensional Mode S.

Nomenclature

$\mathbf{A}$ = vector function (direct problem)
A_j = j th component of vector $\mathbf{A}$
$\mathbf{B}$ = vector function (adjoint problem)
B_j = j th component of vector $\mathbf{B}$
c = phase speed, mode weight
M = Mach number
Pr = Prandtl number
Re = Reynolds number
u = streamwise velocity disturbance
v = normal velocity disturbance
w = spanwise velocity disturbance
x = streamwise coordinate
Y_0 = location of temperature spot
y = normal coordinate
z = spanwise coordinate
a = streamwise wave number
b = spanwise wave number
g = specific heat ratio
q = temperature disturbance
m = viscosity disturbance
p = pressure disturbance
r = density disturbance
w = frequency

Subscripts
e = upper boundary layer edge
p = Laplace transform
sp = saddle point
a = streamwise Fourier transform
b = spanwise Fourier transform

Superscripts
T = transposed
* = dimensional

Introduction

The transition process from laminar to turbulent flow in hypersonic boundary layers has been studied for many years. However, our understanding of this phenomenon is still very poor compared to the low speed case.[1] Several reasons exist for this difference. For example, experimental conditions are severe in hypersonic wind tunnels. Because of high levels of

*Graduate Student, Program in Applied Mathematics.
†Associate Professor, Department of Aerospace and Mechanical Engineering. Senior Member AIAA.

free-stream noise, it is difficult to perform experiments with controlled disturbances, and it is difficult to design perturbers providing high-frequency artificial disturbances of well-controlled characteristics.

Furthermore, interpretation of experimental data is not straightforward, and this issue leads to the need for close coordination between theoretical modeling and experimental design and testing.[2]

Experiments with controlled disturbances could provide insight into the governing mechanisms associated with hypersonic laminar-turbulent transition, with a sharp cone being a good candidate for transition studies due to its relatively simple geometry. Several methods for excitation of artificial disturbances in a hypersonic boundary layer are available. These methods could be used to generate either two-dimensional or three-dimensional wave packets of a broad frequency band.

Additionally, due to advances in computational fluid dynamics, it is possible to perform reliable simulations of laminar-turbulent transition. Ma and Zhong[3,4] and Zhong and Ma[5] have performed direct numerical simulations to better understand the mechanisms leading to hypersonic boundary layer transition.

Accompanying these experiments, both wind-tunnel and numerical, should be theoretical modeling and studies of the development of wave packets in hypersonic boundary layers.

Gustavsson[6] solved a two-dimensional (2D) initial-value problem for incompressible boundary layer flows. Fedorov and Tumin[2] analyzed a 2D initial-value problem in a compressible boundary layer. The problem was solved using a Fourier transform with respect to the streamwise coordinate and a Laplace transform with respect to time. It was shown that the dispersion relation for the discrete spectrum is non-analytic due to the synchronism of the first mode (Mode F) with the entropy and vorticity waves of the continuous spectrum, but the inverse Laplace transform is regular at the synchronism point. Although this regularity ensures that the inverse Fourier transform for the wave packet could be performed, this computation was not done. Forgoston and Tumin[7] extended the work of Ref. 2 by solving the initial-value problem for three-dimensional (3D) wave packets. Once again, the inverse Fourier transform was not computed.

Mack[8,9] used linear stability theory to perform extensive studies of the behavior of 2D and 3D instability modes for both the temporal and spatial problems. In particular, he discovered that for compressible flows, higher acoustic instability modes exist along with the first mode. However, even though the behavior of these modes is understood, the mechanism by which the modes are generated (receptivity problem) is still a subject of research. Throughout the 1980s, 1990s and 2000s, Fedorov and colleagues discovered many results involving the receptivity of high speed flows. One can find a complete bibliography in Ref. 10.

Particularly, this spatial analysis of the 2D instability modes revealed the following: (1) in the region of the leading edge, two discrete modes, Mode F and Mode S, are synchronized with fast and slow acoustic waves respectively; (2) at a downstream location, Mode F is synchronized with the entropy and vorticity waves; (3) farther downstream, Mode F and Mode S also could be synchronized.[11] It is important to understand these features due to the role they may have in the transition process. Later on, similar features of Mode F and Mode S were seen in the 2D temporal problem[2].

For the 3D initial-value problem, Mode F and Mode S was analyzed in Ref. 7 for one particular choice of parameters, and the following features were revealed: (1) the synchronism of Mode S with acoustic waves at low wave number is primarily two-dimensional; (2) at high angles of disturbance propagation, Mode F is no longer synchronized with entropy and vorticity waves; (3) at high angles of disturbance propagation, the synchronism between Mode S and Mode F no longer leads to a Mode S instability, and at even higher angles of disturbance propagation, Mode S and Mode F are not synchronized. A complete understanding of the features of the spectrum is needed to compute the inverse Fourier transform.

We will briefly review the previously solved initial-value problem for a three-dimensional wave packet in a hypersonic boundary layer flow. Our objective is to consider the specific disturbance of an initial temperature spot. The receptivity to the temperature spot is found for both the 2D and 3D cases. The 2D inverse Fourier transform is computed for both Mode F and Mode S. Because of the synchronism of Mode F with entropy/vorticity modes, the path of integration must be deformed around the branch cut that is associated with this synchronism. We show that the computed transform is independent of the path choice. The computed inverse Fourier transform for Mode S is compared with the asymptotic approximation of the Fourier integral. Lastly, we compute the 3D inverse Fourier transform for a prescribed value of the spanwise wave number for Mode S, and we compare this with the asymptotic representation of the Fourier integral.

Problem Formulation

We consider a three-dimensional parallel boundary layer flow of a calorically perfect gas. At the initial time, $t = 0$, a three-dimensional localized disturbance is introduced into the flow. The problem is to

describe the downstream evolution of the perturbation. Denoting

$$\mathbf{A} = \left(u, \partial u/\partial y, v, p, q, \partial q/\partial y, w, \partial w/\partial y\right)^T \qquad (1)$$

as the disturbance vector function, it is possible to rewrite the system of linearized, dimensionless governing equations (continuity equation, x, y and z momentum equations and energy equation) in the following matrix operator form:

$$\frac{\partial}{\partial y}\left(\mathbf{L}_0\frac{\partial \mathbf{A}}{\partial y}\right)+\frac{\partial \mathbf{A}}{\partial y}=\mathbf{H}_{10}\frac{\partial \mathbf{A}}{\partial t}+\mathbf{H}_{11}\mathbf{A}+\mathbf{H}_2\frac{\partial \mathbf{A}}{\partial x}+ \mathbf{H}_3\frac{\partial^2 \mathbf{A}}{\partial x\partial y}+\mathbf{H}_4\frac{\partial^2 \mathbf{A}}{\partial x^2}+\mathbf{H}_5\frac{\partial \mathbf{A}}{\partial z}+\mathbf{H}_6\frac{\partial^2 \mathbf{A}}{\partial x\partial z}+ \mathbf{H}_7\frac{\partial^2 \mathbf{A}}{\partial y\partial z}+\mathbf{H}_8\frac{\partial^2 \mathbf{A}}{\partial z^2} \qquad (2)$$

where $\mathbf{L}_0, \mathbf{H}_{10}, \mathbf{H}_{11}, \mathbf{H}_2, \mathbf{H}_3, \mathbf{H}_4, \mathbf{H}_5, \mathbf{H}_6, \mathbf{H}_7$, and $\mathbf{H}_8$ are 8×8 matrices. The explicit form of these matrices can be found in Ref. 7. At the initial time, $t = 0$, the disturbance vector is denoted as

$$\mathbf{A}(x, y, z, 0) = \mathbf{A}_0(x, y, z) \qquad (3)$$

The boundary conditions are

$$y = 0: \quad u = v = w = q = 0$$
$$y \to \infty: \quad \left|A_j\right| \to 0 \quad (j = 1,...,8) \qquad (4)$$

These boundary conditions correspond to the no-slip condition and zero temperature disturbance on the wall, and all disturbances decaying to zero far outside the boundary layer.

Solution of the Initial-Value Problem

The problem is solved using a Fourier transform with respect to the streamwise coordinate, x, a Fourier transform with respect to the spanwise coordinate, z, and a Laplace transform with respect to time. The inverse Laplace transform of $\mathbf{A}_{pab}$, the solution of the transformed equations, is determined by poles (relevant to the discrete spectrum) and by branch cuts (relevant to the continuous spectrum). By integrating along an appropriate contour in the complex p plane (see Ref. 7), the inverse Laplace transform can be written as a sum of integrals along the sides, g^+ and g^-, of each branch cut and a sum of residues resulting from the poles i.e.

$$\mathbf{A}_{ab} = -\frac{1}{2\pi i}\sum_m\left(\int_{g_m^+}\mathbf{A}_{pab}e^{pt}dp+\int_{g_m^-}\mathbf{A}_{pab}e^{pt}dp\right)+ \sum_n \mathrm{Res}_n\left(\mathbf{A}_{pab}\,e^{pt}\right) \qquad (5)$$

Details of the problem formulation and solution can be found in Ref. 7.

Discrete and Continuous Spectrum

Discrete modes are given by the poles' contribution to the inverse Laplace transform, i.e. the residues shown in Eq. (5). Continuous modes are given by the branch cuts' contribution to the inverse Laplace transform, i.e. the integrals shown in Eq. (5). There are three branch cuts associated with the continuous spectrum. They are shown in Fig. 1 for $a = 0.2$ and $b = 0.14$.

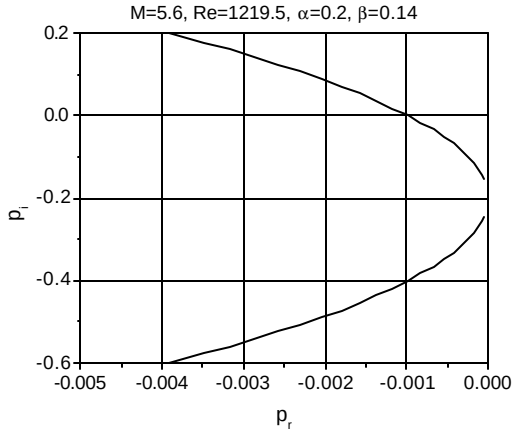

Fig. 1 Branch cuts of the continuous spectrum in the complex plane p.

The upper and lower branch cuts correspond to fast and slow acoustic waves. These waves travel with the respective phase speeds $c = 1 \pm \frac{\sqrt{1 + b^2/a^2}}{M_e}$. The horizontal branch cut contains a region of overlapping vorticity modes as well as a region of entropy disturbances overlapping the two vorticity modes. Both vorticity and entropy waves travel downstream with a phase speed $c = 1$. If an eigenvalue belongs to the discrete spectrum, then the associated eigenfunction decays exponentially outside the boundary layer ($y \to \infty$). Eigenfunctions associated with continuous modes oscillate outside the boundary layer. Details regarding the discrete spectrum and the various regions of the continuous spectrum can be found in Ref. 7.

The behavior of the spectrum must be understood in order to compute the inverse Fourier transform. To illustrate features of the spectrum, we consider a boundary layer over an adiabatic sharp cone at zero angle of attack. The length scale is $L^* = \sqrt{\left(m_e^* x^* / r_e^* U_e^*\right)}$ and the Reynolds number is $Re = \sqrt{\left(r_e^* U_e^* x^* / m_e^*\right)}$. Using the Lees-Dorodnitsyn transformation,[12] we solve the conical problem with boundary layer profiles for a flat plate. Accordingly, all conical results presented hereafter can be adjusted to the flat plate boundary layer by dividing the parameters Re, a, b and w by $\sqrt{3}$. All numerical results are for the case of two-dimensional mean flow. To maintain consistency with the 2D problem analyzed in Ref. 2, we choose the following parameter values: $M = 5.6$, $Re = 1219.5$, $Pr = 0.7$, $g = 1.4$, and stagnation temperature $T_0 = 470K$.

Biorthogonal System of Eigenfunctions

It is possible to express a solution of the initial-value problem as an expansion in the biorthogonal eigenfunction system $\{\mathbf{A}_w, \mathbf{B}_w\}$. The vector $\mathbf{A}_w$ is a solution of the direct problem , and the vector $\mathbf{B}_w$ is a solution of the adjoint problem.

Solutions of the direct and adjoint problems belong to the discrete and continuous spectrum. The eigenfunction system $\{\mathbf{A}_w, \mathbf{B}_w\}$ has an orthogonality relation given as

$$\left\langle \mathbf{H}_{10}\mathbf{A}_w, \mathbf{B}_{w'} \right\rangle \equiv \int_0^\infty \left(\mathbf{H}_{10}\mathbf{A}_w, \mathbf{B}_{w'}\right) dy = \Gamma \Delta_{w,w'} \qquad (6)$$

where Γ is a normalization constant. $\Delta_{w,w'}$ is a Kronecker delta if either w or w' belong to the discrete spectrum. $\Delta_{w,w'} = d\left(w - w'\right)$ is a Dirac delta function if both w and w' belong to the continuous spectrum.

It is possible to show that the inverse Laplace transform can be expressed as an expansion in the biorthogonal eigenfunction system[7]

$$\mathbf{A}_{ab}(y,t) = \sum_n c_n \mathbf{A}_{abw_n}(y) e^{-iw_n t} + \sum_j \int_0^\infty c_j(k) \mathbf{A}_{abw_j}(y) e^{-iw_j(k)t}\, dk \qquad (7)$$

where $\sum_n$ denotes a summation over the discrete spectrum and $\sum_j$ denotes a summation over the continuous spectrum. Using the Fourier transform of the initial disturbance, $\mathbf{A}_{0ab}$, as well as the orthogonality relation (Eq. (6)), one can find the coefficients c_n and c_j. Further details regarding the biorthogonal system of eigenfunctions can be found in Ref. 7.

Receptivity to a Temperature Spot

As an example of a specific initial disturbance, we consider a temperature spot localized at a distance Y_0 from the wall. For the 3D initial-value problem, this disturbance will have the form

$$q(x,y,z) = d(x)d(y - Y_0)d(z) \text{ at } t = 0 \qquad (8)$$

The orthogonality condition given by Eq. (6) allows one to determine the weights of the modes generated by the temperature spot. For Mode F and Mode S, the weight is given by

$$c(a,b) = \frac{\left\langle \mathbf{H}_{10}\mathbf{A}_{0ab}, \mathbf{B}_w \right\rangle}{\left\langle \mathbf{H}_{10}\mathbf{A}_w, \mathbf{B}_w \right\rangle} \qquad (9)$$

where $w(a,b)$ corresponds to the eigenvalue for the mode of interest. For a temperature spot of the form given by Eq. (8), one obtains from Eq. (9) the expression

$$c(a,b) = \frac{H_{10}^{35}(Y_0)\mathbf{B}_{w3}(Y_0) + H_{10}^{65}(Y_0)\mathbf{B}_{w6}(Y_0)}{\left\langle \mathbf{H}_{10}\mathbf{A}_w, \mathbf{B}_w \right\rangle} \qquad (10)$$

with H_{10}^{ij} denoting the (i, j) element of matrix $\mathbf{H}_{10}$.

The denominator of Eqs. (9,10) is an arbitrary normalization constant. In the following analysis, we have chosen to normalize the eigenfunction $\mathbf{A}_w$ as $u_{\max}$ = inner maximum of $u(y) = 1$. With this normalization, c is the amplitude of the maximum streamwise velocity component $u_{\max}$ associated with the appropriate mode.

As a limiting case, as $b \to 0$, one obtains the receptivity coefficient associated with the 2D initial-value problem.[2]

Inverse Fourier Transform-2D

The 2D inverse Fourier transform is given by

$$\int_{-\infty}^{\infty} c(a)\,\mathbf{A}(a,y)\,e^{i(ax-w(a)t)}\,da \qquad (11)$$

As an example, we consider the streamwise velocity component, u, of the disturbance vector, $\mathbf{A}$. The transform we are therefore interested in is given as

$$\int_{-\infty}^{\infty} c(a)\,u(a,y)\,e^{i(ax-w(a)t)}\,da \qquad (12)$$

where the coefficient $c(a)$ is, for this example, the amplitude of the maximum streamwise velocity component $u_{\max}$. Eq. (12) is transformed using a symmetry argument. Using the direct and adjoint matrix operator equations, when a is replaced by $-a$, i.e. when $a \to -a$, it can be shown that $w \to \overline{w}$, $c \to \overline{c}$ and $u \to \overline{u}$, where the overbar stands for complex conjugate. Therefore, Eq. (12) can be rewritten as

$$\begin{aligned}\int_{-\infty}^{\infty} c(a)\,u(a,y)\,e^{i(ax-w(a)t)}\,da = \\ \int_{0}^{\infty} c(a)\,u(a,y)\,e^{i(ax-w(a)t)}\,da + \\ \int_{0}^{\infty} \overline{c}(a)\,\overline{u}(a,y)\,e^{-i(ax-\overline{w}(a)t)}\,da = \\ 2\int_{0}^{\infty} \mathrm{Real}\left\{c(a)\,u(a,y)\,e^{i(ax-w(a)t)}\right\}da\end{aligned} \qquad (13)$$

In the computation, we ignore the factor of 2. For the purpose of analysis, we shall consider Mode F and Mode S separately.

Mode F

Figure 2 shows the imaginary part of the eigenvalue w_i for Mode F. Figure 3 shows the maximum streamwise velocity amplitude $u_{\max}$ for Mode F, which is generated by a components of the temperature spot located at varying normal distances Y_0 from the wall.

We numerically compute the integral given by Eq. (13) from $a = 0.1$ to $a = 0.5$. We were unable to calculate the Mode F eigenvalues below $a \approx 0.08$ (Fig. 2). However, the input into the integral for $a = 0.0$ to $a = 0.1$ is not significant since the receptivity coefficient, $u_{\max}$, is close to 0 for this range of a (Fig. 3).

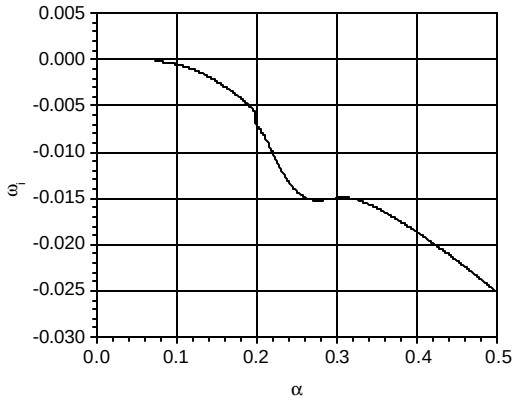

Fig. 2 Imaginary part of eigenvalue for Mode F.

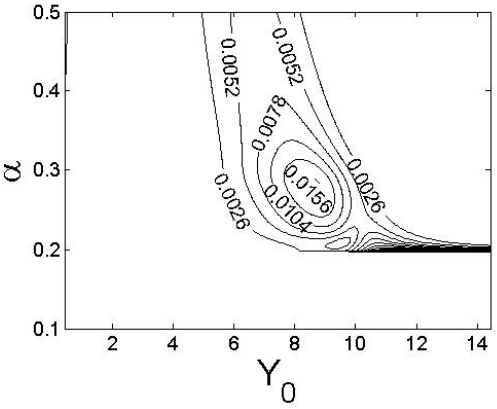

Fig. 3 Contours of $u_{\max}$ generated by a components of the temperature spot located at Y_0.

Fig. 3 also shows that the largest values of $u_{\max}$ occur near $a \approx 0.3$. This fact, coupled with the fact that Mode F is everywhere decaying, suggests that there will not be much input into the integral for $a > 0.5$ if a sufficiently large time, t, is chosen.

There is a synchronism between Mode F and the entropy and vorticity modes of the phase speed $c = 1$. As the discrete mode coalesces with the continuous spectrum from one side of the branch cut, it reappears on the other side at another point. This leads to a jump in w_i.

Figure 4 shows contours of w_i in the complex a plane. One can see the jumps in w_i along a nearly vertical line. Since these jumps are associated with a branch cut, as we integrate Eq. (13) from $a = 0.1$ to $a = 0.5$, we must deform the path of integration

around the branch cut. Figure 5 is a schematic of an integration path chosen to avoid the branch cut.

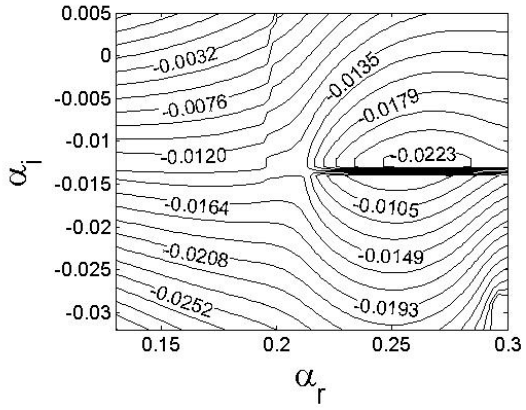

Fig. 4 Contours of w_i in the complex a plane.

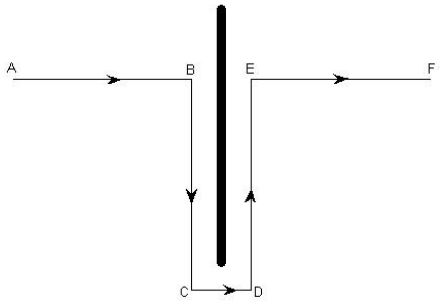

Fig. 5 Schematic of an integration path around the branch cut.

Due to analyticity of the function being integrated, the result should be independent of the path of integration.

Using $Y_0 \approx 9.0$, $t = 50$ and the integration path, Path 1, Eq. (13) is integrated. Using the letters found in Fig. 5, Path 1 is given explicitly as the following: At point A, $a = 0.1$. At point B, $a = 0.17$. At point C, $a = 0.17 - 0.015i$. At point D, $a = 0.2 - 0.015i$. At point E, $a = 0.2$, and at point F, $a = 0.5$.

The result is shown in Figure 6 as contours of u in the $x - y$ plane. To better illustrate the Mode F wave packet, Figure 7 shows a slice of Fig. 6 taken at $y = 2.02$.

One can see that the wave packet shown in Fig. 7 has a well defined periodic structure, with period of about 21. The wave number corresponding to this period is given as $2p/21 = 0.299$. At this short time, the main input into the integral is from the receptivity coefficient, and we expect the wave number that corresponds to the period of the wave packet to be near the value of a for which $u_{\max}$ is a maximum. In fact, for our choice of $Y_0 = 8.9$, $u_{\max}$ attains its largest value at $a = 0.297$, which compares favorably with $a = 0.299$.

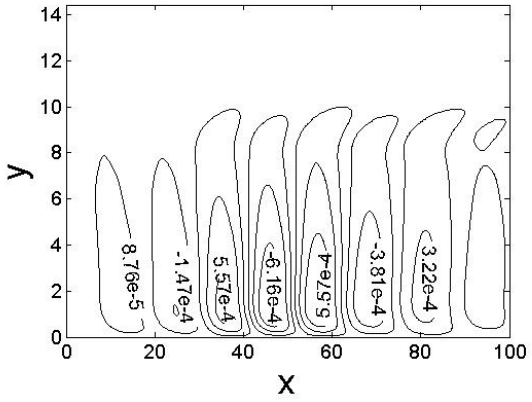

Fig. 6 Contours of u in the x - y plane.

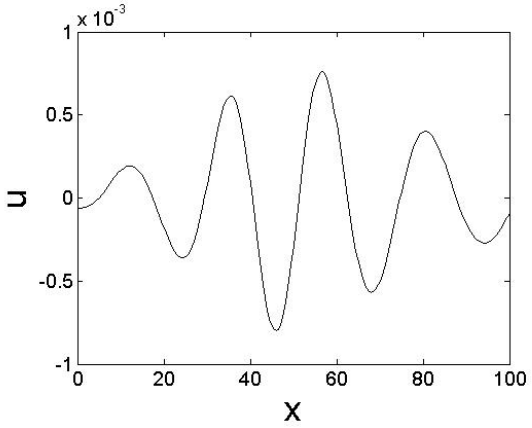

Fig. 7 Streamwise velocity disturbance, u, at y = 2.0207 for t = 50.

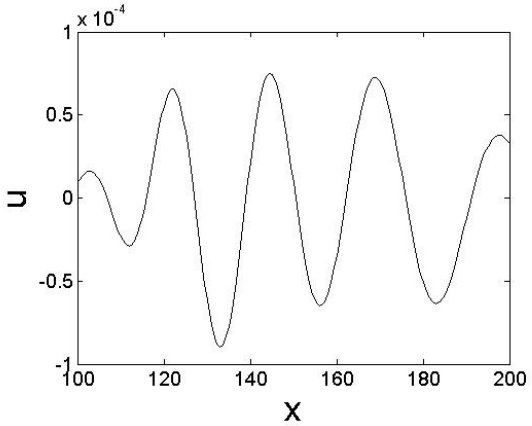

Fig. 8 Streamwise velocity disturbance, u, at y = 2.02 for t = 200.

To illustrate the decay of the wave packet in time, Eq. (13) is integrated again using Path 1 and $Y_0 = 8.9$ for $t = 200$. Figure 8 shows the result taken at the slice $y = 2.02$.

When Fig. 8 is compared to Fig. 7, one sees that u is an order of magnitude smaller for $t = 200$ than for $t = 50$. Additionally, the wave packet is seen to have moved downstream with the increase in time.

To ensure that these results are independent of the choice of path of integration, the results shown for $Y_0 = 8.9$ at $t = 50$ using Path 1 are compared with results found using three other paths of integration. Using the letters found in Fig. 5, Paths 2,3 and 4 are given as follows:

Path 2 - At point A, $a = 0.1$. At point B, $a = 0.15$. At point C, $a = 0.15 - 0.015i$. At point D, $a = 0.2 - 0.015i$. At point E, $a = 0.2$, and at point F, $a = 0.5$.

Path 3 - At point A, $a = 0.1$. At point B, $a = 0.15$. At point C, $a = 0.15 - 0.015i$. At point D, $a = 0.21 - 0.015i$. At point E, $a = 0.21$, and at point F, $a = 0.5$.
Path 4 - At point A, $a = 0.1$. At point B, $a = 0.17$. At point C, $a = 0.17 - 0.031i$. At point D, $a = 0.2 - 0.031i$. At point E, $a = 0.2$, and at point F, $a = 0.5$.

To compare the results, Figure 9 shows the wave packet at the slice $y = 2.02$ for each choice of integration path.

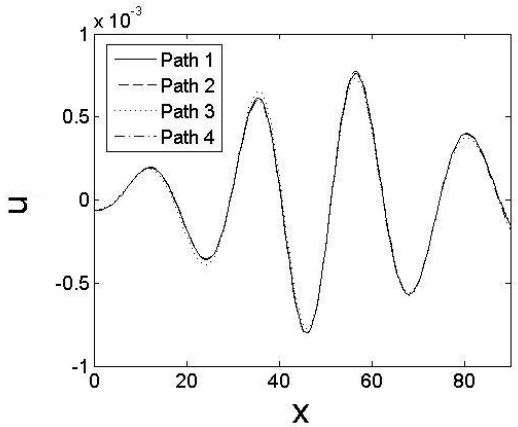

Fig. 9 Streamwise velocity disturbance, u, at $y = 2.02$ for $t = 50$ for 4 paths of integration.

There is good agreement between the results obtained using the four different integration paths. Since a portion of each path of integration passes through a region of the complex a plane where $a_i < 0$, there is numerical error downstream of the wave packet. This error is associated with growth from the e^{iax} term in the integrand. Since Path 3 has a longer portion of its path in the negative complex a plane, this phenomena also explains why the Path 3 result differs slightly from the other three results.

Mode S

Figure 10 shows the imaginary part of the eigenvalue w_i for Mode S. Figure 11 shows the maximum streamwise velocity amplitude u_{max} for Mode S, which is generated by a components of the temperature spot located at varying normal distances Y_0 from the wall.

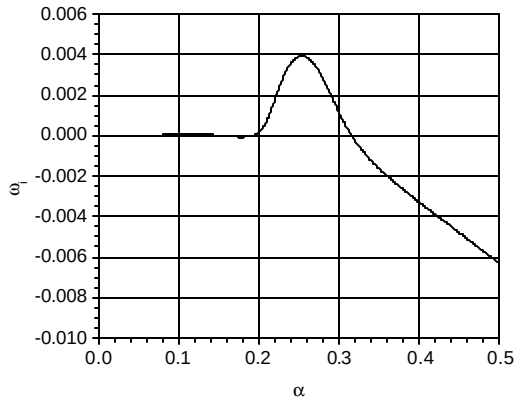

Fig. 10 Imaginary part of eigenvalue for Mode S.

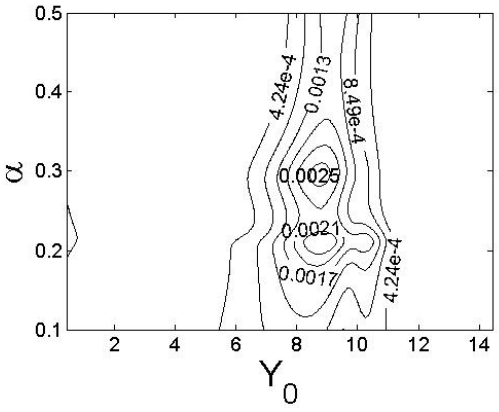

Fig. 11 Contours of u_{max} generated by a components of the temperature spot located at Y_0.

We numerically compute the integral given by Eq. (13) from $a = 0.1$ to $a = 0.5$. The greatest input into the integral will be from the region of $a \approx 0.2$ to $a \approx 0.3$. It is in this region that the receptivity coef-

ficient, $u_{\max}$, is the highest, and it is also in this region where w_i attains its largest value. Beyond $a = 0.5$, Mode S is decaying, so that for sufficiently large times, there will not be significant input into the integral for $a > 0.5$.

Unlike the Mode F case, there is no need to deform the path of integration to compute the Mode S inverse Fourier transform. The result for $Y_0 = 8.9$ at $t = 500$ is shown in Figure 12 as contours of u in the $x-y$ plane.

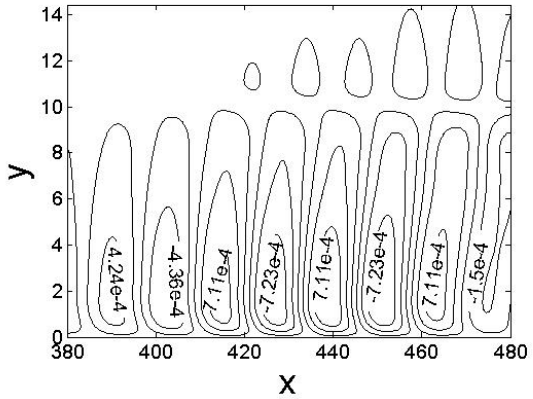

Fig. 12 Contours of u in the x - y plane.

To better illustrate the Mode S wave packet, Figure 13 shows a slice of Fig. 12 taken at $y = 2.02$.

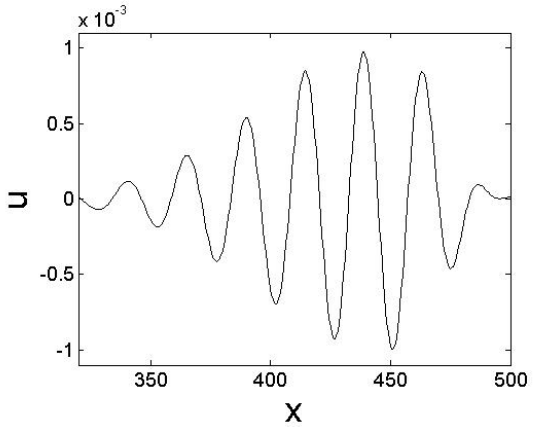

Fig. 13 Streamwise velocity disturbance, u, at $y = 2.02$ for $t = 500$.

The wave packet shown in Fig. 13 has a well defined periodic structure, with period of about 24. The wave number corresponding to this period is given as $2p/24 = 0.262$. The main input into the integral comes from the Gaussian shaped portion of the Mode S eigenvalue plot (Fig. 10). The peak of the Gaussian occurs at $a = 0.254$, which compares favorably with $a = 0.262$.

Because the eigenvalue plot for Mode S contains a region where $w_i > 0$, the Mode S wave packet, unlike the Mode F wave packet, will grow in time (and downstream). Since this behavior is relevant to the transition process, it is useful to compare the Mode S computed inverse Fourier transform with an asymptotic approximation of the Fourier integral.

The development of two and three-dimensional wave packets comprised of spatially growing discrete modes for boundary layer flows (parallel and non-parallel) has been considered previously by Gaster.[13,14,15] In particular, Gaster used the method of steepest descent to find the asymptotic representation of integrals of the form given by Eq. (13). Starting with Eq. (13), we have the following

$$\int c(a)u(a,y)e^{i(ax-w(a)t)}da = \int c(a)u(a,y)e^{it\left(a\frac{x}{t}-w(a)\right)}da \tag{14}$$

Assuming that the saddle point lies near the point $a_{\max}$, we approximate $w(a)$ as follows

$$w(a) = w_{\max} + (a-a_{\max})\left(\frac{\partial w}{\partial a}\right)_{\max} + \frac{1}{2}(a-a_{\max})^2\left(\frac{\partial^2 w}{\partial a^2}\right)_{\max} \tag{15}$$

where $\left(\frac{\partial w}{\partial a}\right)_{\max}$ is real valued.

To find the saddle point, a_{sp}, at a prescribed x/t, we let $j(a) = ax/t - w(a)$ and derive the following

$$\left(\frac{\partial j}{\partial a}\right)_{sp} = \frac{x}{t} - \left(\frac{\partial w}{\partial a}\right)_{\max} - (a_{sp}-a_{\max})\left(\frac{\partial^2 w}{\partial a^2}\right)_{\max} = 0 \tag{16}$$

Solving for a_{sp}, one obtains

$$a_{sp} = a_{\max} + \frac{\frac{x}{t} - \left(\frac{\partial w}{\partial a}\right)_{\max}}{\left(\frac{\partial^2 w}{\partial a^2}\right)_{\max}} \tag{17}$$

Equation (17) can be rewritten as

$$a_{sp} = a_{max} + \frac{x - x_{max}}{t\left(\frac{\partial^2 w}{\partial a^2}\right)_{max}} \qquad (18)$$

where $x_{max} = t\left(\frac{\partial w}{\partial a}\right)_{max}$.

Equation (14) can now be rewritten as

$$c(a_{sp})u(a_{sp},y)\int_L e^{it\left(j(a_{sp})+\frac{1}{2}(a-a_{max})^2 j''(a_{sp})\right)}da =$$

$$c(a_{sp})u(a_{sp},y)\sqrt{-\frac{2p}{itj''(a_{sp})}}e^{itj(a_{sp})} =$$

$$c(a_{sp})u(a_{sp},y)\sqrt{\frac{2p}{it\left(\frac{\partial^2 w}{\partial a^2}\right)_{max}}}e^{itj(a_{sp})} \qquad (19)$$

where L is the contour of integration that has been deformed to pass through the saddle point.

After substitution of a_{sp} into Eq. (19), we obtain the asymptotic representation of the original Fourier integral

$$c(a_{sp})u(a_{sp},y)\sqrt{\frac{2p}{it\left(\frac{\partial^2 w}{\partial a^2}\right)_{max}}}\times$$

$$\exp\left(ia_{max}x + \frac{i(x-x_{max})^2}{2t\left(\frac{\partial^2 w}{\partial a^2}\right)_{max}} - iw_{max}t\right) \qquad (20)$$

Actually, the use of a 2nd order Taylor series expansion of $w(a)$ within the framework of the method of steepest descent is equivalent to Gaster's[13,14] Gaussian model for a Fourier integral.

Using numerical results, the various quantities found in Eq. (20) can be determined. They are

$a_{max} = 0.254$, $w_{max} = 0.2342 + 0.0039i$,

$\left(\frac{\partial w}{\partial a}\right)_{max} = 0.86$ and

$\left(\frac{\partial^2 w}{\partial a^2}\right)_{max}$ = -0.2034 - 3.6431i .

Additionally, $c(a)u(a,y)$, the receptivity coefficient multiplied by the eigenfunction at the saddle point for the slice $y = 2.02$ is 0.00174-0.0011i .

These values can be used to compare the computed inverse Fourier transform with the asymptotic approximation of the transform. The computation gives the "exact" shape of the wave packet, while the asymptotic approximation is derived using a 2nd order Taylor series. Though we expect good agreement between the two methods, especially for large times, there may be some differences between the "exact" result found numerically and the "approximate" result found with the method of steepest descent.

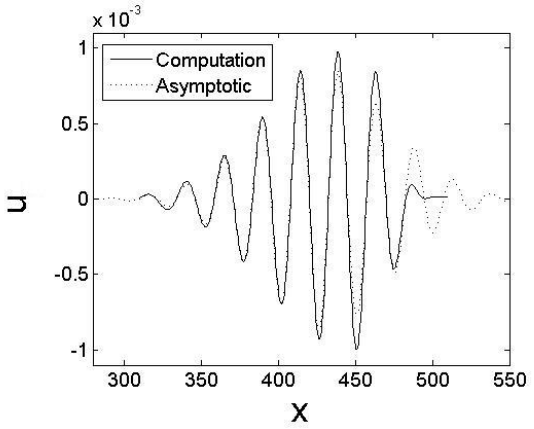

Fig. 14 Comparison of computed integral with the asymptotic approximation for t = 500 .

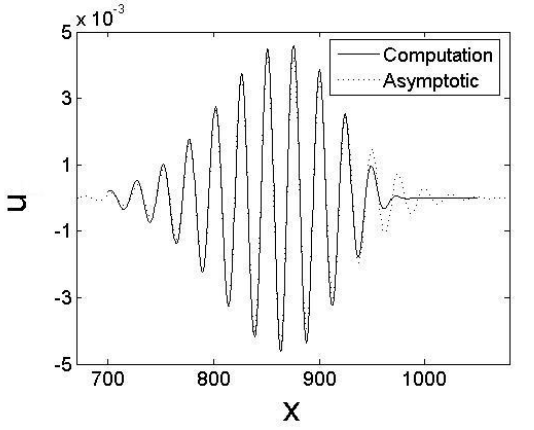

Fig. 15 Comparison of computed integral with the asymptotic approximation for t = 1000 .

Figure 14 compares the wave packet found for $Y_0 = 8.9$ and $t = 500$ at the slice $y = 2.02$ with the

asymptotic approximation at $t = 500$ given by Eq. (20) using the values given above. Figures 15 and 16 show similar comparisons for $t = 1000$ and $t = 1500$ respectively.

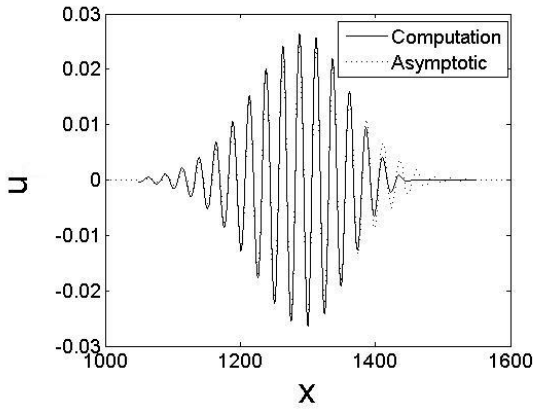

Fig. 16 Comparison of computed integral with the asymptotic approximation for $t = 1500$.

One can see that the asymptotic representation provides a good approximation to the computation at $t = 500$, and that as time progresses, the two wave packets have even better agreement with each other. One can also see that as time increases, the wave packet spreads out as it moves downstream. Furthermore, the amplitude of the perturbation increases with time.

Inverse Fourier Transform-3D

For the streamwise velocity disturbance, u, the 3D inverse Fourier transform is now given by

$$\int_{-\infty}^{\infty}\int_{-\infty}^{\infty} c(a,b)u(a,b,y)e^{i(a\,x+b\,z-w(a,b)t)}da\;db \tag{21}$$

For a prescribed b, Eq. (21) becomes

$$e^{ibz}\int_{-\infty}^{\infty} c(a,b)\,u(a,b,y)e^{i(a\,x-w(a,b)t)}da \tag{22}$$

As for the 2D case, the integral of Eq. (22) can be transformed using a symmetry argument to an integral over the positive a half-plane. As before, for the purpose of computation, we ignore the factor of 2. The asymptotic approximation of the 3D inverse Fourier transform for prescribed b is

$$c(a_{sp},b)u(a_{sp},b,y)\sqrt{\frac{2p}{it\left(\frac{\partial^2 w}{\partial a^2}\right)_{max}}}\exp(ibz)\times$$
$$\exp\left(ia_{max}x+\frac{i(x-x_{max})^2}{2t\left(\frac{\partial^2 w}{\partial a^2}\right)_{max}}-iw_{max}t\right) \tag{23}$$

Mode S

Figure 17 shows the imaginary part of the eigenvalue w_i for Mode S for $b = 0.1001$. Using numerical results, the various quantities found in Eq. (23) can be determined. They are

$a_{max} = 0.259$, $w_{max} = 0.2396 + 0.0030i$,

$\left(\frac{\partial w}{\partial a}\right)_{max} = 0.88$ and

$\left(\frac{\partial^2 w}{\partial a^2}\right)_{max} = 0.1056 - 3.4483i$.

Additionally, $c(a,b)u(a,b,y)$, the receptivity coefficient multiplied by the eigenfunction at the saddle point for the slice $y = 2.02$ is 0.00159-0.00126i.

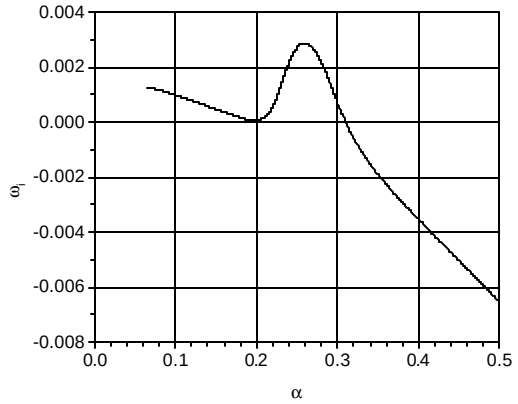

Fig. 17 Imaginary part of eigenvalue for Mode S for $b = 0.1001$.

Figure 18 shows for Mode S the maximum streamwise velocity amplitude $u_{\max}$ multiplied by the value of the eigenfunction at $y = 2.02$, which is generated by a and b components of the temperature spot located at the distance $Y_0 = 8.9$ from the wall.

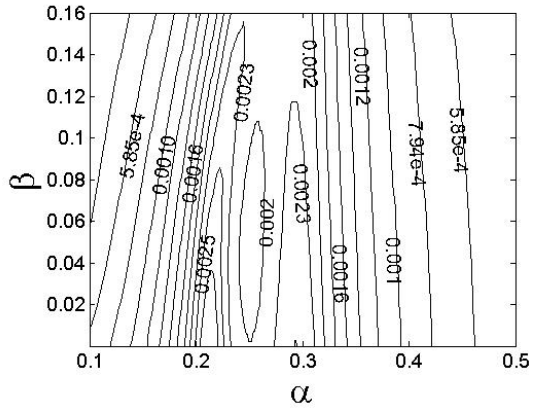

Fig. 18 Contours of $c(a,b)u$ at $y = 2.02$ generated by a and b components of a temperature spot located at $Y_0 = 8.9$.

We numerically compute the inverse Fourier transform from $a = 0.1$ to $a = 0.5$ with $b = 0.1001$ and $z = 0$. Even though $w_i > 0$ for $a < 0.1$, the receptivity coefficient (Fig. 18) is near 0 in this region. Once again, the greatest input into the integral will be from the region of $a \approx 0.2$ to $a \approx 0.3$. It is in this region that the receptivity coefficient, $u_{\max}$, is the highest, and it is also in this region where w_i attains its largest value. Beyond $a = 0.5$, Mode S is decaying, so that for sufficiently large times, there will not be significant input into the integral for $a > 0.5$.

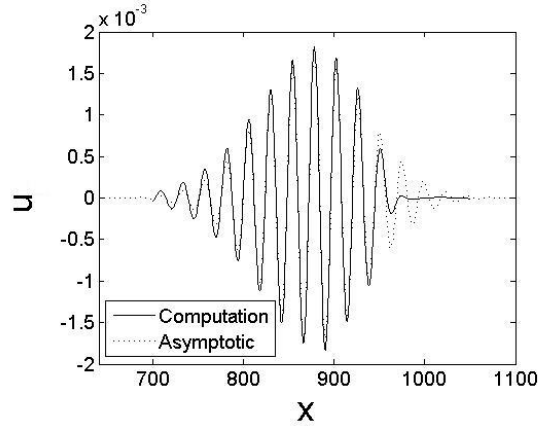

Fig. 19 Comparison of computed integral with the asymptotic approximation for $b = 0.1001$, $z = 0$ and $t = 1000$.

Figure 19 compares the wave packet found for $b = 0.1001$, $z = 0$, $Y_0 = 8.9$ and $t = 1000$ at the slice $y = 2.02$ with the asymptotic approximation at $t = 1000$ given by Eq. (23).

As another example, Figure 20 shows the imaginary part of the eigenvalue w_i for Mode S for $b = 0.1401$.

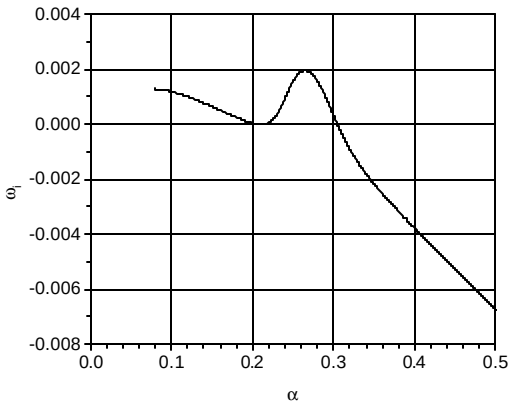

Fig. 20 Imaginary part of eigenvalue for Mode S for $b = 0.1401$.

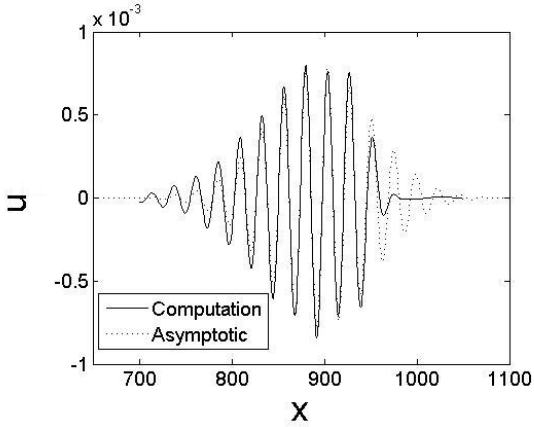

Fig. 21 Comparison of computed integral with the asymptotic approximation for $b = 0.1401$, $z = 0$ and $t = 1000$.

Using numerical results, the following quantities are found

$a_{\max} = 0.265$, $w_{\max} = 0.2446 + 0.0021\mathrm{i}$,

$\left(\frac{\partial w}{\partial a}\right)_{\max} = 0.90$ and

$\left(\frac{\partial^2 w}{\partial a^2}\right)_{\max} = -0.2245 - 3.1321\mathrm{i}$.

$c(a,b)u(a,b,y)$ at the saddle point for the slice $y = 2.02$ is 0.00162-0.00135i .

Figure 21 compares the wave packet found for $b = 0.1401$, $z = 0$, $Y_0 = 8.9$ and $t = 1000$ at the slice $y = 2.02$ with the asymptotic approximation at $t = 1000$.

Conclusions

In this paper, we used the previously solved 2D and 3D initial-value problems along with features of the spectrum for one case of parameters to study the evolution of wave packets for two discrete modes, Mode S and Mode F.

Given the specific disturbance of an initial temperature spot, we computed the 2D inverse Fourier transform for both Mode F and Mode S. The results for Mode S were compared with the asymptotic approximation of the Fourier integral. The 3D inverse Fourier transform was also computed for Mode S for prescribed values of the spanwise wave number b. The results lead to the following conclusions:

1) Due to the synchronism between Mode F and entropy/vorticity waves, the path of integration must be deformed around the branch cut associated with this synchronism. Since the integrand is analytic, the choice of the integration path should not affect the result, and in fact, the numerical results for four choices of integration path agree very well.

2) The asymptotic approximation found using the method of steepest descent provides very good agreement with the computed inverse Fourier transform for sufficiently large time. This is true both for the 2D Fourier integral and the 3D Fourier integral with prescribed b.

Future work will include the computation of the 3D inverse Fourier transform for a range of b.

Acknowledgments

The authors would like to thank the National Science Foundation for providing a VIGRE graduate student fellowship to E.F.

References

[1]Reshotko, E., "Boundary Layer Instability, Transition and Control," *AIAA Paper* 94-0001, Jan. 1994.

[2]Fedorov, A., Tumin, A., "Initial-Value Problem for Hypersonic Boundary-Layer Flows," *AIAA Journal*, Vol. 41, No. 3, March 2003, pp. 379-389.

[3]Ma, Y., Zhong, X., "Receptivity of a supersonic boundary layer over a flat plate. Part 1. Wave structures and interactions," *Journal of Fluid Mechanics*, Vol. 488, 2003, pp. 31-78.

[4]Ma, Y., Zhong, X., "Receptivity of a supersonic boundary layer over a flat plate. Part 2. Receptivity to free-stream sound," *Journal of Fluid Mechanics*, Vol. 488, 2003, pp. 79-121.

[5]Zhong, X., Ma, Y., "Receptivity and Linear Stability of Stetson's Mach 8 Blunt Cone Stability Experiments," *AIAA Paper* 2002-2849, June 2002.

[6]Gustavsson, L.H., "Initial-value problem for boundary layer flows," *Physics of Fluids*, Vol. 22, No. 9, 1979, pp. 1602-1605.

[7]Forgoston, E., Tumin, A. "Initial-Value Problem for Three-Dimensional Disturbances in a Hypersonic Boundary Layer," *AIAA Paper* 2004-2243, June 2004.

[8]Mack, L. M., "Boundary-Layer Stability Theory," Jet Propulsion Lab., JPL 900-277, Pasadena, CA, Nov. 1969.

[9]Mack, L.M., "Special Course on Stability and Transition of Laminar Flow," Paper reprinted from AGARD Report 709, June 1984.

[10]Fedorov, A.V., "Receptivity of a high-speed boundary layer to acoustic disturbances," *Journal of Fluid Mechanics*, Vol. 491, 2003, pp. 101-129.

[11]Fedorov, A.V., Khokhlov, A.P., "Prehistory of Instability in a Hypersonic Boundary Layer," *Theoretical and Computation Fluid Dynamics*, Vol. 14, 2001, pp. 359-375.

[12]Anderson, Jr., J.D., *Hypersonic and High Temperature Gas Dynamics*, AIAA, Inc., Reston, Virginia, 1989.

[13]Gaster, M., "Propagation of Linear Wave Packets in Laminar Boundary Layers," *AIAA Journal*, Vol. 19, No. 4, April 1981, pp. 419-423.

[14]Gaster, M., "The Development of a Two-Dimensional Wavepacket in a Growing Boundary Layer," Proc. Royal Soc. London, Vol. 384, No. 1787, Dec. 1982, pp. 317-332.

[15]Gaster, M., "The development of three-dimensional wave packets in a boundary layer," *Journal of Fluid Mechanics*, Vol. 32, 1968, pp. 173-184.